Influence of Secondary Reactions on the Heat of Pyrolysis of Biomass

ARTICLE *in* INDUSTRIAL & ENGINEERING CHEMISTRY RESEARCH · DECEMBER 2009

Impact Factor: 2.59 · DOI: 10.1021/ie9007985

4 AUTHORS, INCLUDING:

Federica Barontini
Università di Pisa
55 PUBLICATIONS **920** CITATIONS
SEE PROFILE

Enrique Velo
Polytechnic University of Catalonia
87 PUBLICATIONS **1,030** CITATIONS
SEE PROFILE

Influence of Secondary Reactions on the Heat of Pyrolysis of Biomass

Claudia Gomez,[†] Enric Velo,[†] Federica Barontini,[‡] and Valerio Cozzani*[,§]

Centre d'Enginyeria de Processos i Medi Ambient (CEPIMA), Universitat Politècnica de Catalunya, Avenida Diagonal 647, 08028 Barcelona, Spain, Dipartimento di Ingegneria Chimica, Chimica Industriale e Scienza dei Materiali, Università degli Studi di Pisa, via Diotisalvi 2, 56126 Pisa, Italy, and Dipartimento di Ingegneria Chimica, Mineraria e delle Tecnologie Ambientali, Alma Mater Studiorum - Università di Bologna, via Terracini 28, 40131 Bologna, Italy

The thermal behaviors during the pyrolysis of two different biomass samples, beech wood from carpentry residuals and artichoke thistle from energy-dedicated crops, were investigated. Thermogravimetry/differential scanning calorimetry (TG-DSC) and thermogravimetry coupled to Fourier transform infrared (TG-FTIR) analysis of evolving products were used to investigate the thermal effects of the pyrolysis process. The role of pretreatments (hot-water washing, ethanol extraction, and their combination) was also analyzed. High alterations in the heat demand were observed as a function of the initial sample mass and pyrolysis conditions. The role of vapor−solid secondary interactions was evidenced by the evolution profiles of the main pyrolysis products.

1. Introduction

The need for sustainable energy sources is growing as the availability of fossil energy sources is diminishing. In the past few years, there has been a renewed interest in biomass as a potential supplier of useful energy and chemicals, with a reduced environmental impact compared to fossil fuels.[1−12] Pyrolysis and other thermochemical conversion processes represent an important option for energy recovery from biomass and waste. The upsurge of interest in the simulation and optimization of reactors for thermochemical processes requires appropriate models that integrate different operating conditions and different feedstocks, helping to achieve a better understanding of the reactions in the corresponding processes.[13−31]

The heat of reaction has a significant influence on thermal conversion routes, and understanding the effect of the reaction heat is important in the modeling of thermochemical processes. However, the thermal effects of pyrolysis reactions have been found to vary widely, ranging from exothermic to endothermic under different operating conditions.[32,33] Secondary reactions between volatiles and char, as well as autocatalytic effects due to impurities, are usually assumed to be the reasons for the wide variation of values reported in the literature for the heat requirements of the pyrolysis process. In fact, in several reactors proposed for slow pyrolysis and gasification on an industrial scale, a relevant contact time is present among volatiles generated in the primary pyrolysis process and the primary char.[2,34,35]

Under slow pyrolysis conditions, small particles of cellulose and wood show a global endothermic behavior, whereas samples with larger particle sizes exhibit exothermic behaviors.[36] This difference was explained in terms of the enhanced interaction of hot pyrolysis vapors with the decomposing solid, which involves an exothermic reaction that leads to the formation of char. Mok et al.[37] observed a linear relationship between reaction exothermicity and char yield. The yield of charcoal is also known to be favored by the presence of some mineral elements in biomass ash.[32] Inorganic ions are known to exert a great influence on the thermal degradation of the natural polymers (polysaccharides and lignin) that make up biomass materials.[38] The extractive content of samples is a further factor affecting the thermal and kinetic behavior of the pyrolysis process.[15,16,39,40] However, to the knowledge of the authors, no data have been reported in the literature concerning the impact of sample pretreatments on the thermal effects of the pyrolysis process.

In previous studies, the pyrolysis of biomass feedstocks that represent a waste disposal problem and/or that have substantial energy and chemical potential was investigated.[41,42] In particular, previous investigations focused on the thermal behavior of woody samples coming from the carpentry industry and on raw material from energy crops (artichoke thistle) in Spain. The kinetic description of the primary decomposition process of these samples was provided, assuming a low heat demand coming from the thermal effects due to pyrolysis reactions.

In the present study, the actual heat demand during the pyrolysis of these materials was investigated by differential scanning calorimetry (DSC). In the experimental runs, untreated, water-washed, and ethanol-extracted samples were used, as well as samples subjected to both water washing and ethanol extraction. Experimental runs involving thermogravimetry combined with DSC (TG-DSC) were also carried out, influencing the contact time available for vapor−solid secondary interactions. The profiles of volatile compounds formed during TG pyrolysis experimental runs, obtained by online FTIR analysis, were also analyzed, in an effort to better understand the effect of vapor−solid interactions on the composition of the evolved products.

2. Experimental Section

2.1. Materials. Artichoke thistle (*Cynara cardunculus*) from a specialized crop in the Spanish province of Soria was used as a reference material, representing a herbaceous biomass that is currently used for energy production in some European regions. The samples were milled to a fine powder. A washing treatment was applied to obtain samples having a lower content of mineral matter.[41] Table 1 reports the ultimate and proximate analyses of untreated and washed samples.

* To whom correspondence should be addressed. Tel.: (+39)-051-2090240. Fax: (+39)-051-2090247. E-mail: valerio.cozzani@unibo.it.
[†] Universitat Politècnica de Catalunya.
[‡] Università degli Studi di Pisa.
[§] Alma Mater Studiorum - Università di Bologna.

10.1021/ie9007985 CCC: $40.75
Published on Web 10/26/2009

Table 1. Proximate and Ultimate Analyses of the Sample Materials Used in the Study

Proximate Analysis (% by weight)				
biomass	moisture	volatile matter	fixed carbon	ash
untreated beech	7.03	73.62	19.11	0.24
washed beech	2.35	79.05	18.40	0.20
untreated thistle	11.10	63.39	17.41	8.10
washed thistle	2.43	70.79	22.01	4.77

Ultimate Analysis (% by weight; dry ash-free samples)				
biomass	C	H	N	O
untreated beech	45.68	6.52	<0.10	47.80
washed beech	47.43	6.55	<0.10	46.02
untreated thistle	40.45	6.07	1.08	52.40
washed thistle	45.04	6.70	0.97	47.29

Additional thistle samples were obtained applying an extraction treatment and a combined washing and extraction treatment by the procedures described in detail in a previous publication.[41] The content of extractives of the thistle samples was determined to be 6.1% by weight.

To provide a comparison with a ligneous biomass material, beech chips from carpentry residues were used. In a few experimental runs, washed beech samples were also used. The ultimate and proximate analyses of these materials are also included in Table 1.

2.2. Techniques and Procedures. DSC experimental data were obtained using a Mettler DSC 25 calorimeter. Experimental runs were performed using pure nitrogen as the purge gas (gas velocity of ~0.005 m/s). Typical total sample weights of about 2−10 mg were used. All samples were dried at a temperature of 110 °C for 30 min before the experimental runs. To provide the proper contact between the sample and the sample holder, each sample was pressed into a disk having a diameter of 5 mm and a height of about 1.3 mm. The DSC runs were performed using aluminum crucibles. Depending on the desired experimental conditions, the crucible was used without a lid (thus resulting in a 5-mm-diameter surface available for mass transfer to the gas flow) or with a pierced lid (thus limiting the surface available for mass transfer to a 1-mm-diameter hole). A preliminary calibration of the DSC instrument was performed using the heat of fusion of a known quantity of indium.

Simultaneous thermogravimetric and DSC data were obtained using a Netzsch STA 409/C thermoanalyzer. Samples in crucibles both with and without lids were used. Runs were carried out using a pure nitrogen gas flow of 60 mL/min and aluminum crucibles. Also in this case, samples were dried at a temperature of 110 °C for 30 min and were pressed into disks having a 5-mm diameter before the experimental runs.

FTIR measurements were carried out using a Bruker Equinox 55 spectrometer equipped with a mercury-cadmium-telluride (MCT) detector. TG-FTIR simultaneous measurements were carried out by coupling the FTIR spectrometer to the Netzsch TG using a 2-mm-internal-diameter Teflon tube. The 800-mm-long transfer line and the head of the TG balance were heated at a constant temperature of 200 °C to limit the condensation of volatile decomposition products. FTIR measurements were carried out with an MCT detector in a specifically developed low-volume gas cell (8.7 mL) with a 123-mm path length, heated at a constant temperature of 250 °C. The gas flow from the TG outlet to the IR gas cell had a rate of 60 mL/min, and a residence time of 30 s in the transfer line could be evaluated for the evolved gases. This value was assumed as the time delay correction to be used for the comparison of TG and IR results. During TG-FTIR runs, spectra were collected at 4 cm^{-1} resolution, with coaddition of 16 scans per spectrum. This resulted in a temporal resolution of 9.5 s, which is more than sufficient to follow the gas evolution rates characteristic of TG runs at heating rates of 20 °C/min. FTIR data were used to calculate specific emission profiles following the procedures discussed in section 2.4.

Table 2. Wavenumber Ranges Used for the Determination of Emission Profiles

wavenumber range (cm^{-1})	assignment
2240−2400	CO_2
2143−2236	CO
1660−1820	C═O stretching
2600−3150	C−H stretching

All experimental runs were started at a temperature of 75 °C. A constant heating rate of 20 °C/min was used up to the final temperature of the run, which was set at 550 °C. At the end of each run, the furnace was cooled to ambient temperature while a nitrogen purge gas flow was maintained. The heating rate was selected well in the range of those allowed by the available TG and DSC devices (the maximum heating rate is 50 °C/min, and the minimum heating rate for practical reasons is 5 °C/min). A preliminary screening of the influence of the heating rate and a comparison with the results of a previous study[33] indicated that no relevant influence of the heating rate is present for values ranging between 5 and 50 °C/min.

The char formed in DSC runs was weighed, and a second run was performed on the char sample using the same experimental conditions (temperature range and heating rate). All of the DSC results reported in this study were corrected by baselines obtained from runs with empty crucibles. The resulting experimental heat flows from the biomass samples are denoted as Q_{run}, whereas the heat flow data from the residual char are identified as Q_{char}.

2.3. Experimental Determination of the Heat of Pyrolysis. To achieve quantitative data on the heat of reaction during the pyrolysis process from the DSC curves, it was necessary to obtain reasonable reference lines. For this purpose, the approach of Rath et al.[33] was used. Each heat flow curve obtained from DSC measurements was thus considered as the sum of two components: the heat flow necessary to heat the sample (due to the thermal inertia of the sample) and the heat of reaction. To separate the first effect from the second, a theoretical heat flow curve for sample heating was calculated from available specific heat and sample conversion experimental data. A dimensionless sample conversion was defined as

$$X(T) = \frac{m_0 - m_T}{m_0 - m_{char}} \tag{1}$$

where m_0 is the initial sample weight, m_T is the sample weight at temperature T, and m_{char} is the final weight of the solid product of the pyrolysis process (called "char" in the following discussion). The values of m_0 and m_{char} were assumed to be constants in eq 1 and in the subsequent equations. The heat flow curve, Q_s, was thus estimated as

$$Q_s = [1 - X(T)]Q_{bio,s} + X(T)Q_{char,s} \tag{2}$$

where

$$Q_{bio,s} = m_0 c_{p,bio} \frac{dT}{dt} \tag{3}$$

and

$$Q_{\mathrm{char,s}} = m_{\mathrm{char}} c_{\mathrm{p,char}} \frac{\mathrm{d}T}{\mathrm{d}t} \tag{4}$$

In eqs 2−4, dT/dt is the heating rate (20 °C/min), m_{char} is the weight of the solid sample at the end of the pyrolysis process (when $X = 1$), and c_{p} is the specific heat calculated according to formulas given in the literature[33] for the biomass ($c_{\mathrm{p,bio}}$) and for the char ($c_{\mathrm{p,char}}$). Q_{s} represents the heat flow necessary to heat the sample without considering the thermal effects of the pyrolysis reaction. Thus, in the absence of other complicating phenomena, the heat flow due to thermal effects of the reaction, Q_{r}, can be estimated subtracting Q_{s} from the baseline-corrected experimental DSC heat flow curve, Q_{run}.

Previous studies reported that the presence or absence of a lid can have a significant effect on both the shape and the apparent baseline of the heat flow curve.[33,43] The effect on the baseline was recognized to be the effect of radiative heat exchange, because of the different emissivity of the sample compared to that of the empty crucible in runs without a lid.[43] If crucibles without lids are used, the influence of heat radiation effects must also be considered. In this work, the radiative heat,

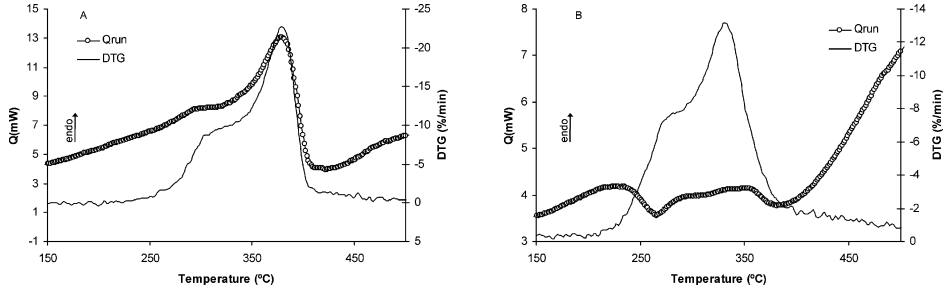

Figure 1. DTG and DSC data obtained in pyrolysis runs for (A) untreated beech and (B) untreated thistle samples. Conditions: Pure nitrogen, 20 °C/min, crucibles without lids, 6-mg initial sample weight.

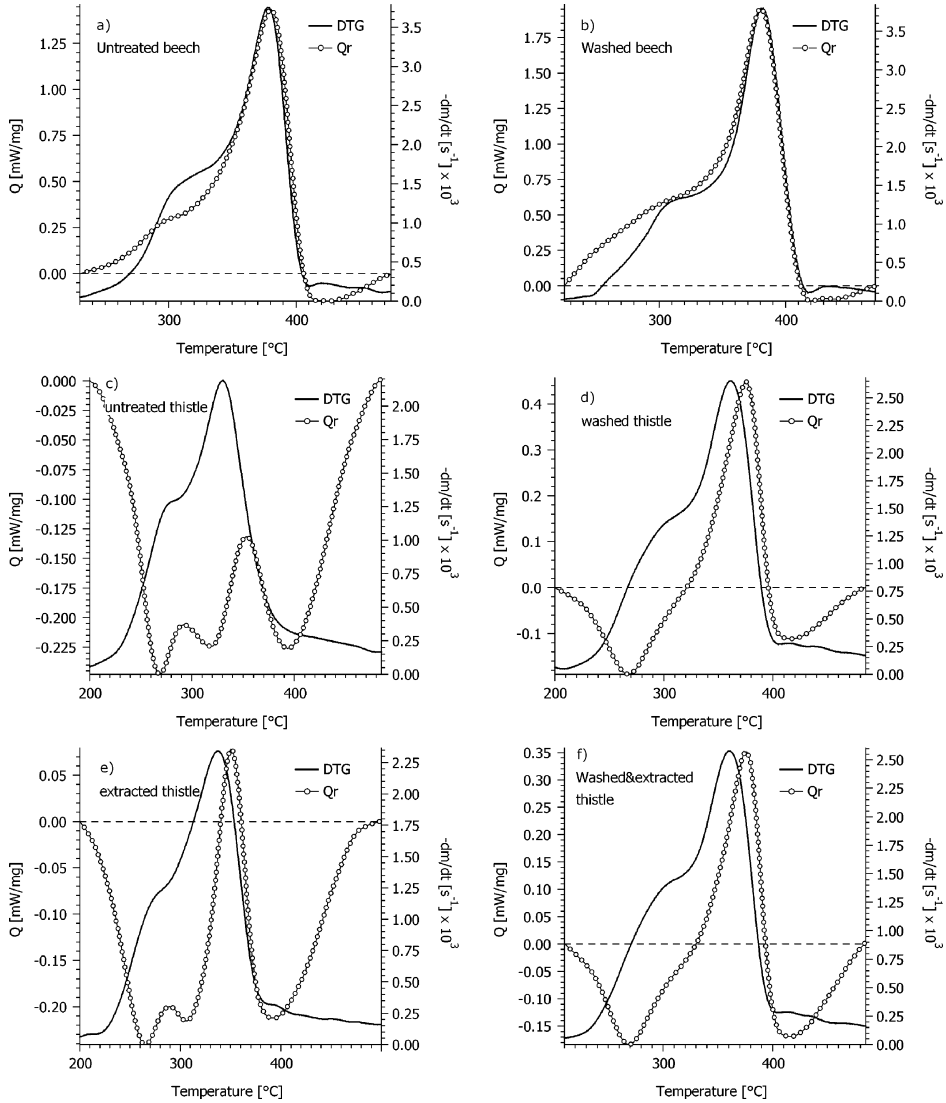

Figure 2. DTG and heat flow data obtained in pyrolysis runs for untreated and pretreated samples of biomass. Conditions: Pure nitrogen, 20 °C/min, crucibles without lids, 6-mg initial sample weight. Negative values of Q correspond to exothermic behavior.

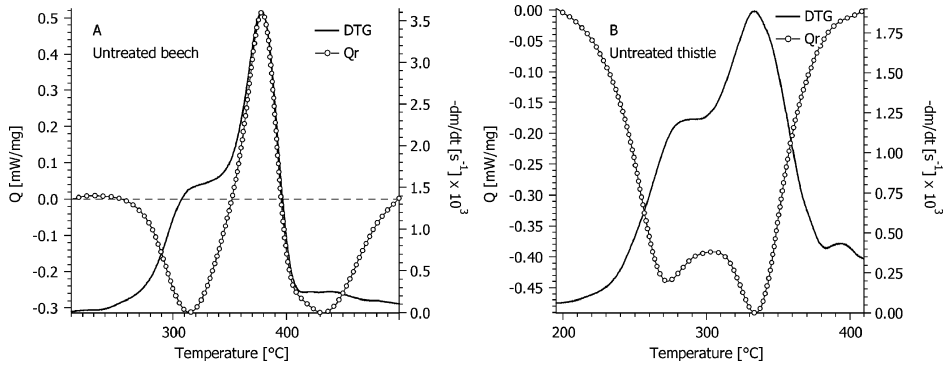

Figure 3. DTG and heat flow data obtained in pyrolysis runs for untreated samples of biomass. Conditions: Pure nitrogen, 20 °C/min, crucibles with lids, 6-mg initial sample weight. Negative values of Q correspond to exothermic behavior.

Q_{rad}, was calculated as the difference between the calculated $Q_{char,s}$ (eq 4) and the experimental heat flow from the residual char, Q_{char}.

The same procedure was used to obtain the reaction heat curve from the DSC results in the presence of a pierced lid. However, in these runs, radiation heat flow effects did not need to be considered.[43] Thus, the Q_{rad} correction was not required in these cases, and only Q_s was subtracted from the experimental Q_{run} curve.

The total heat of pyrolysis, H_{total}, was then calculated from a numerical integration as

$$H_{total} = \frac{1}{m_0}\int_{T_1}^{T_2} Q_r \, dt \tag{5}$$

where T_1 and T_2 are the initial and final temperatures, respectively, of the decomposition process. These temperatures vary for each sample depending on the characteristics of the differential thermogravimetric (DTG) curves and were assumed as the onset temperatures of the DTG peak.

2.4. Evolved Gas Analysis. Qualitative gas evolution profiles of volatile species released in TG-FTIR runs were obtained from the experimental data following a procedure described extensively elsewhere.[44] The procedure uses an integral form of the Lambert−Beer law over a selected wavenumber interval

$$I = \int_{\tilde{\nu}_1}^{\tilde{\nu}_2} A(\tilde{\nu})\, d\tilde{\nu} = c\int_{\tilde{\nu}_1}^{\tilde{\nu}_2} \varepsilon(\tilde{\nu}) l \, d\tilde{\nu} = Kc \tag{6}$$

where A is the measured absorbance, I is the integral value, ε is the extinction coefficient of the gaseous compound, l is the optical path length used in the measurement, c is the concentration, $(\tilde{\nu}_1, \tilde{\nu}_2)$ is the wavenumber interval selected for the measurement, and K is a constant.

Even in the absence of an experimental calibration, eq 6 shows that TG-FTIR measurements can be used to generate a specific gas profile to monitor qualitatively the evolution of a gas as a function of the time or of the temperature of the TG furnace. This requires the availability of a wavenumber absorption interval of the chemical species of interest that is free of additional contributions from other substances. The simultaneous formation of a wide number of volatile compounds complicates the selection of such intervals. The wavenumber ranges used for the determination of the emission profiles are presented in Table 2. Absorptions due to C−H stretching vibrations were associated with aliphatic and aromatic compounds. Signals due to C═O stretching vibrations were associated with carbonyl and carboxyl functional groups (e.g., aldehydes, ketones, acids, esters).

Specific data on the total quantities of the different products evolved in TG-FTIR runs could be obtained by integration of eq 6 with respect to time, which gives

$$D = \int_{t_1}^{t_2}\left[\int_{\tilde{\nu}_1}^{\tilde{\nu}_2} A(\tilde{\nu})\, d\tilde{\nu}\right] dt = \int_{t_1}^{t_2} Kc \, dt \tag{7}$$

where (t_1, t_2) is the interval in which the chemical species of interest passes through the FTIR sampling cell. The value of integral D is directly related to the total amount of the species of interest evolved during the (t_1, t_2) interval.[44,45] Even in the absence of an experimental calibration, the integral in eq 7 (called FTIR area in the following discussion) allows for the assessment of specific trends in the yields of the different volatile pyrolysis products.

3. Results and Discussion

3.1. Results of DSC Runs. The thermal effects of the primary decomposition process of the untreated and pretreated samples were investigated by DSC experimental runs. The analysis started from a comparison of the results of DSC runs in crucibles without lids, because the absence of a lid in the presence of a purge gas flow (pure nitrogen) promotes the rapid evaporation of primary volatiles, thus reducing secondary interactions between the solid residue and the volatiles. Figure 1 compares the raw DSC and DTG data for samples of untreated beech and thistle, each with an initial weight of 6 mg. The characteristics of the DTG curves of these samples were discussed in detail in earlier studies.[42] As shown in Figure 1A, the peak in the DSC curve and the peak in the differential weight loss curve match for the beech sample. The two curves have similar shapes, and the pyrolysis process exhibits clear endothermic behavior for this sample. A more complex behavior is shown by the herbaceous crop, as is evident from Figure 1B.

Figure 2 shows the heat flow curves due to the reaction thermal effects, Q_r, obtained by subtracting the sum of Q_{rad} and Q_s from the baseline-corrected experimental DSC heat flow curve, Q_{run}. All of the data reported in the figures were derived from the analysis of three different experimental runs. A considerable agreement (less than 2% error) was found among different experimental runs performed on the same sample material.

Processing the DSC data by this procedure allowed for the observation of a second exothermic peak in the untreated wood sample at temperatures between 405 and 475 °C. An exothermic peak in the same temperature range was also identified during the thermal decomposition of spruce at similar heating rates.[33] The presence of an exothermic peak can be explained by the decomposition of lignin, which is the most important precursor

Table 3. Values of the Heat Required by the Pyrolysis Process in Crucibles without Lids

type of wood	char yield	H_{total}[a] (J g^{-1})
untreated thistle	0.34	−132.7
extracted thistle	0.31	−122.2
washed thistle	0.26	−37.5
washed and extracted thistle	0.26	−23.8
untreated beech	0.17	222.2

[a] Values correspond to arithmetic averages from repeated experiments.

Table 4. Values of the Heat Required by the Pyrolysis Process in Crucibles with Lids

type of wood	char yield	H_{total}[a] (J g^{-1})
untreated thistle	0.36	−178.5
extracted thistle	0.34	−170.1
washed thistle	0.29	−142.6
washed and extracted thistle	0.30	−111.8
untreated beech	0.22	−67.6

[a] Values correspond to arithmetic averages from repeated experiments.

of char in the pyrolysis process. As shown in the figure, the water-washed sample exhibited a higher endothermic heat flow, which might be associated with the lower mineral matter content and, consequently, with the lower rate of char formation in this sample.

In the case of the herbaceous crop, the heat flow of the untreated sample fell completely in the exothermic region. Local shoulders can be observed between 270 and 400 °C, during the main decomposition step (see Figure 2c). The corresponding heat flow curve for the water-washed thistle sample noticeably approaches the shape of the DTG curve, becoming similar to that of beech wood, as shown by a comparison of parts b and d of Figure 2. The extraction also leads to a shift of the heat flow curve toward endothermicity, although by a minor extent, as shown in Figure 2e. Nevertheless, the thermal decomposition of thistle starts and ends with exothermic stages that fall inside the wide temperature range of lignin decomposition. The endothermic behavior becomes increasingly important between 270 and 395 °C, which is within the main range of devolatilization of the holocellulose content. The temperature of the heat flow peak is slightly above the occurrence of the peak of the DTG curve for the herbaceous crop. The endothermic maxima (around 350 °C in the untreated thistle and 370 °C for the pretreated samples) are coincident with the DTG peaks of the partial reaction associated with cellulose decomposition in an earlier kinetic study of this biomass.[42]

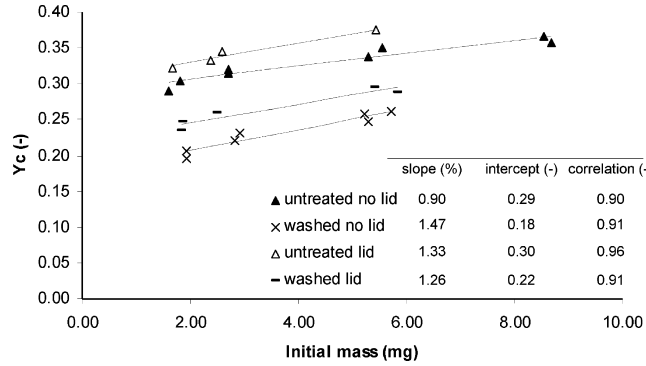

Figure 5. Char yield as a function of initial mass for untreated and washed thistle, in crucibles with and without lids. Data in the table correspond to linear correlations. Percentages are expressed with respect to the initial sample weight.

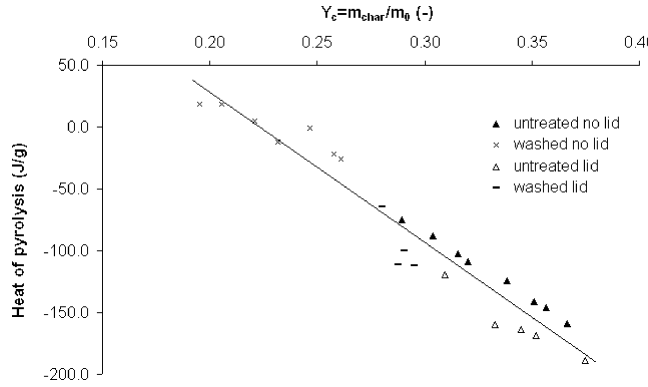

Figure 6. Heat of pyrolysis as a function of char yield for untreated and washed thistle samples having different initial weight in crucibles with and without lids. Linear regression: slope = −1211.9 J/g, intercept = 270.3 J/g, regression coefficient = 0.933.

Table 3 reports the values calculated for the heats of pyrolysis and the final char yields (solid residue at 550 °C) obtained in DSC runs. Whereas the thermal decomposition of the herbaceous crop is dominated by exothermic phenomena, the decomposition of beech samples exhibited a highly endothermic behavior. However, the endothermic effects during the pyrolysis of these samples were far lower than those of pure cellulose (ranging between 560 and 710 J/g[46]). Thus, the present results are well within the range of those obtained in previous studies[33] and confirm the findings of Stenseng et al.[46] As shown in Table 3,

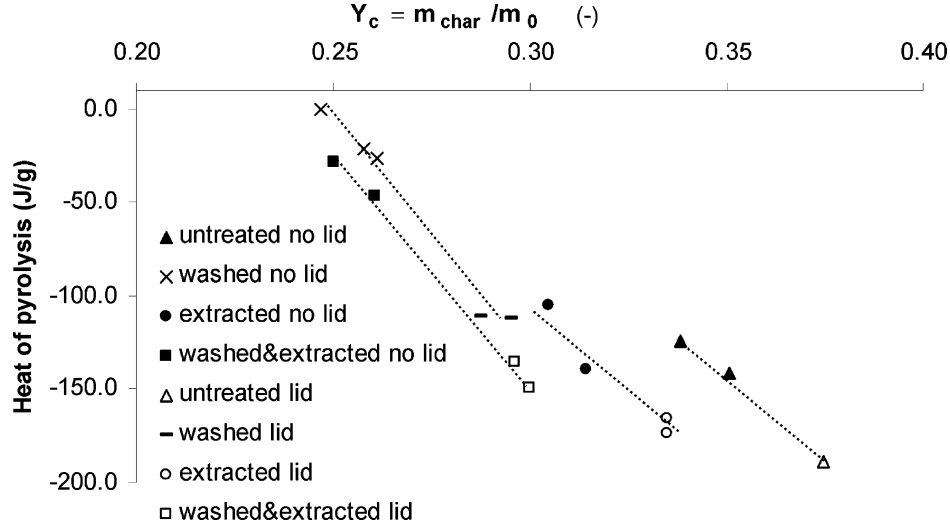

Figure 4. Heat of pyrolysis as a function of char yield for untreated and pretreated 6-mg thistle samples, in crucibles with and without lids.

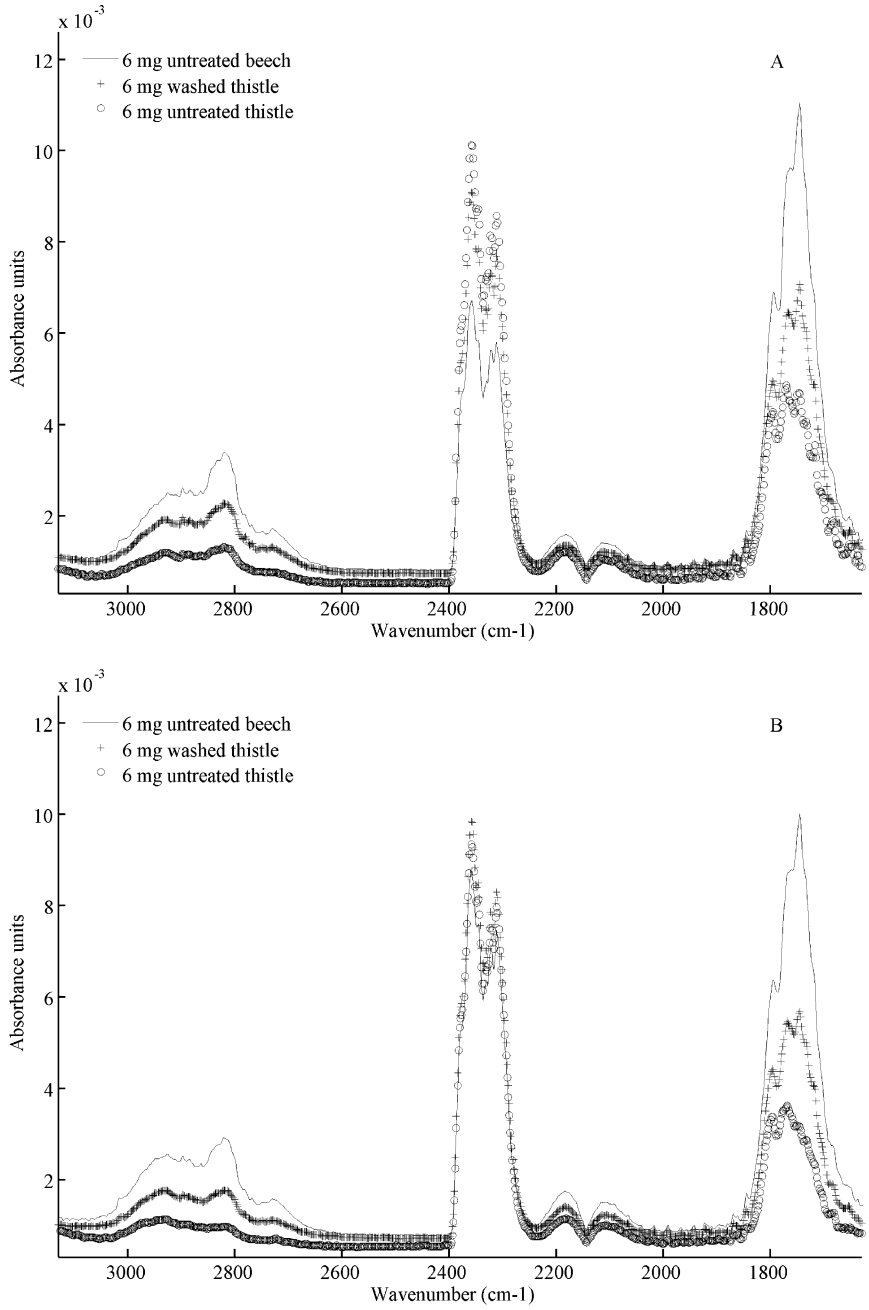

Figure 7. Comparison between FTIR spectra recorded during the pyrolysis of 6-mg untreated beech, untreated thistle, and washed thistle samples, at the temperature of maximum devolatilization, using (A) uncovered and (B) covered pans. Intensities have been normalized by the initial sample weight.

the pretreatments increase the endothermic character of the process. The results also show that water washing causes higher variations in the thermal effects of the pyrolysis process than does the extraction process. An increase of up to 95.2 J/g in the heat demand was found after water washing, whereas an increase of only 10.5 J/g in the heat demand was found after extraction. Table 3 also indicates that a clear correspondence is present between an increase of the endothermicity and a decrease of the char yield.

The highest differences in char yield and overall thermal effects are between the untreated thistle sample and the untreated beech sample. Even after the partial elimination of the inorganic and extractive components, the thermal effects associated with thistle pyrolysis are less endothermic than those of the beech sample. The higher amount of lignin present in the herbaceous crop, and thus the higher content of holocellulose in wood, might well justify these differences.

3.2. Influence of Secondary Gas−Solid Interactions on DSC Results. To enhance gas−solid interactions (secondary pyrolysis process), additional sets of experimental runs were carried out, with modification of two experimental parameters: the surface available for the mass transfer of volatiles to the nitrogen purge stream and the initial weight of the sample.

In a first set of experimental runs, samples having the same initial weight (6 mg) and crucibles with punctured lids were used. The presence of a punctured lid above the DSC crucible limited the surface available for mass transfer to that of a hole, present in the crucible lid, having a 1-mm diameter. Although this is the standard procedure used to prepare samples for experimental runs with crucibles at atmospheric pressure, previous studies indicated that these conditions enhance interactions among the solid residue and the volatiles formed in the pyrolysis process.[33]

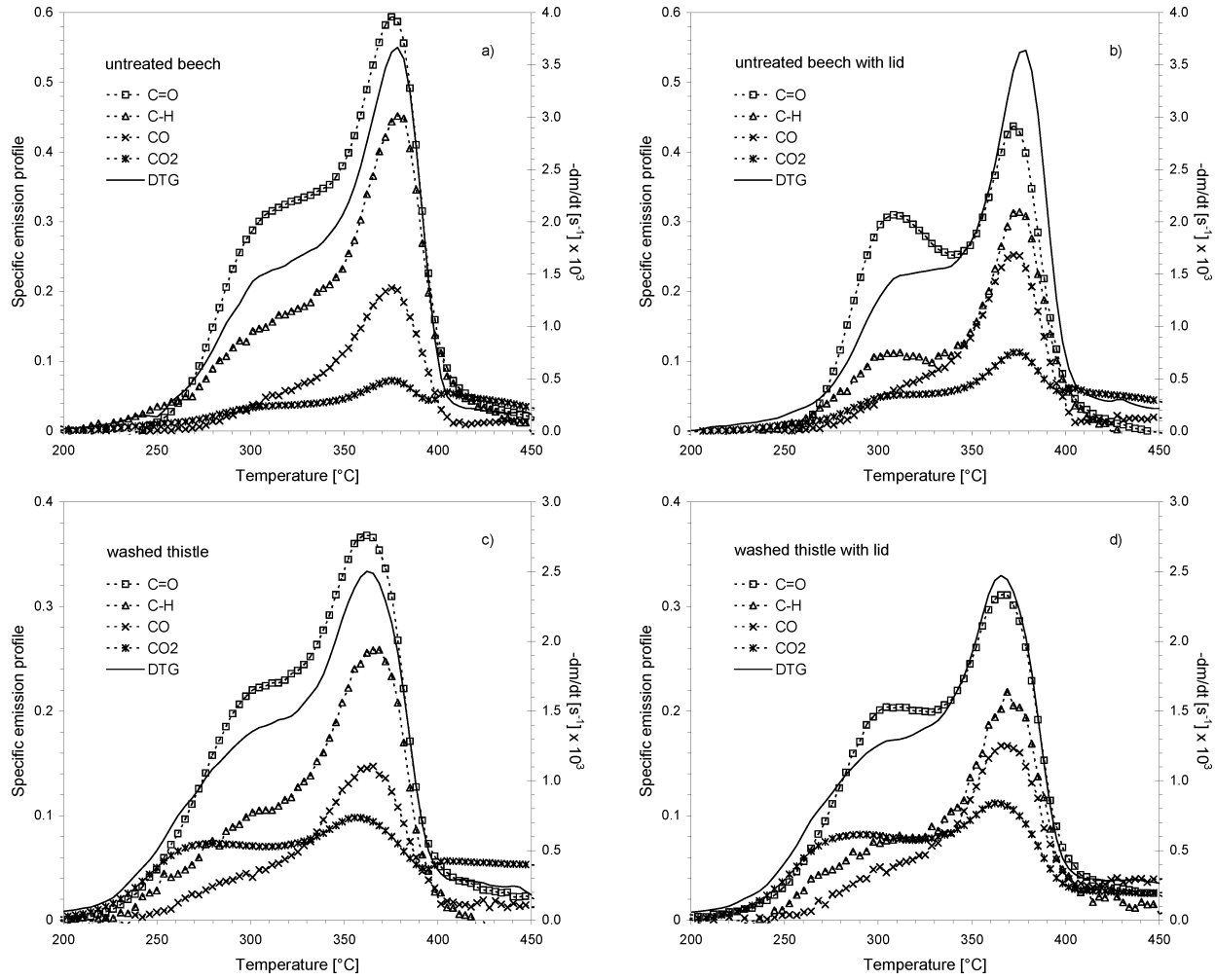

Figure 8. DTG data and volatile product evolution profiles obtained during the pyrolysis of untreated beech and washed thistle at 20 °C/min, using crucibles with and without lids (6-mg initial sample weight). The scaling factors for the individual functionalities evolved from wood and thistle are the same.

The procedure described in section 2.3 was applied to obtain the Q_r curves shown in Figure 3. For the wood sample, an exothermic effect appears to prevail at the beginning of the decomposition. As shown by a comparison of Figures 2a and 3A, the last exothermic stage (between 405 and 475 °C) is far more pronounced than in the case of DSC runs carried out without lids. Also, in the case of thistle, higher overall exothermic effects are recorded (see Figure 3). The numerical values calculated for the overall heat of the pyrolysis process, reported in Table 4, confirm these observations.

Figure 4 shows the heat of pyrolysis calculated for untreated and pretreated thistle samples as a function of the char yield obtained for runs with and without lids. As shown in the figure, linear trends (straight dotted lines) are present among the overall heat and the final char yield. Correlation coefficients were found to be above 0.94 for all of the materials. Thus, for all of the samples analyzed, a higher char yield always corresponded to a higher exothermicity (or lower endothermicity) of the overall pyrolysis process. This suggests that the higher residence time of primary volatiles in the vicinity of the solid residue enhances exothermic secondary char formation reactions.

The lines that represent the correlation between char yields and pyrolysis thermal effects shift toward lower exothermic effects with increasing effectiveness of the pretreatment. For example, given the char yield, the strongest exothermic effects with respect to char yield were recorded for the untreated sample; lower values were recorded for the sample obtained after extraction, and the sample obtained after extraction and water washing exhibited the lowest exothermicity with respect to the char yield.

The slopes of the trend lines are very similar for the two washed samples. Furthermore, the slopes are higher than those corresponding to the untreated and extracted samples, suggesting that the washed samples are more strongly affected by the enhancement of gas−solid interactions caused by the presence of a lid.

An additional set of experiments was carried out with the initial sample weight varied in the range between 2 and 10 mg, including runs both with and without a lid. Variations in the initial sample weight resulted in further limited changes in the final char yield, in accordance with previous findings.[33] Figure 5 shows the variation of the char yield as a function of the initial sample weight. As shown in the figure, increasing the initial sample weight in the mentioned range resulted in an increase in the char yield of up to 8%. Also in this case, the increase in the final char yield can be attributed to the enhancement of secondary interactions among the primary volatiles and the solid residue, because of the higher contact times for samples having higher initial weights.

The increase in the final char yield was associated with an increase in the exothermicity of the overall decomposition process. Figure 6 summarizes the data obtained for the overall heat of pyrolysis under all experimental conditions and for all samples used in the present study. The heat of pyrolysis is

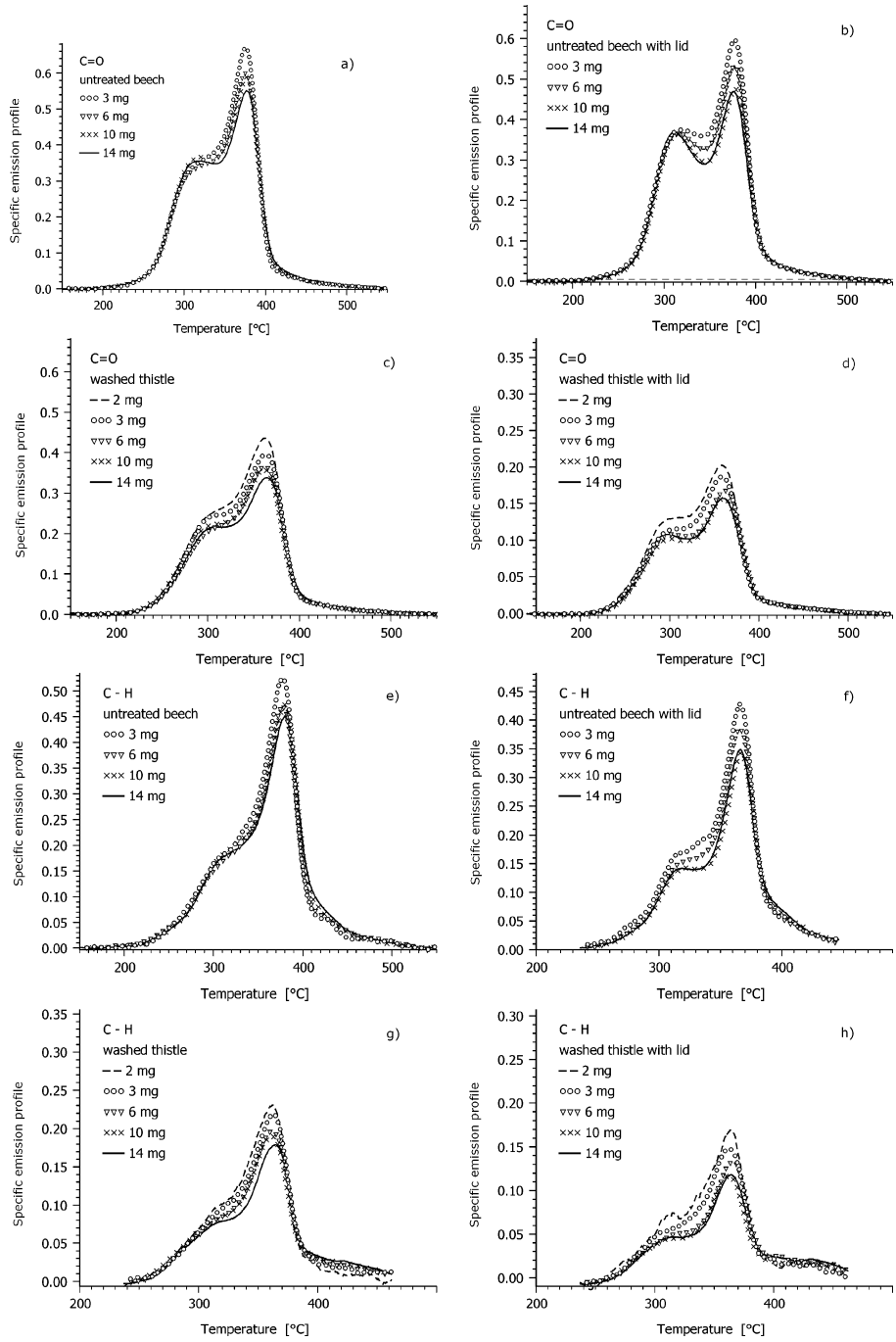

Figure 9. Organic product evolution profiles during the pyrolysis of untreated beech and washed thistle at 20 °C/min, using crucibles with and without lids. Results for samples having different initial weights are also reported. The scaling factors for the individual functionalities evolved from wood and thistle are the same.

reported as a function of the final char yield. As shown in the figure, the heat of pyrolysis is highly affected by the final char yield. In the case of thistle samples, the overall heat of pyrolysis increased from an endothermic value of 20 J/g to an exothermic value of −200 J/g for char yields between 20% and 40%. The figure shows that a linear correlation can reasonably approximate the trend of the experimental data. This supports the assumption that exothermic interactions among primary volatiles and residual solid leading to secondary char formation can strongly influence the overall thermal effects of the pyrolysis process.

3.3. Influence of Secondary Gas−Solid Interactions on Volatile Evolution. To better understand the role of secondary interactions between volatiles and the solid residue, the evolved gas was analyzed. TG-DSC-FTIR experimental runs were performed under the same conditions used for the DSC runs discussed in the preceding sections.

The characterization of volatile products of biomass pyrolysis by TG-FTIR analysis can be complicated by a variety of effects. Whereas simple chemical species (e.g., CO and CO_2) can be detected easily, organic compounds can hardly be identified, because of the simultaneous evolution of a high number of species. Thus, in the present work, organic pyrolysis products were lumped on the basis of the presence of functional groups, following an approach developed in previous studies.[44,47]

Typical infrared spectra of the volatiles evolved during the TG-FTIR pyrolysis runs carried out on the investigated biomass samples are shown in Figure 7. In this figure, the FTIR spectra recorded in correspondence to the DTG peak in the decomposi-

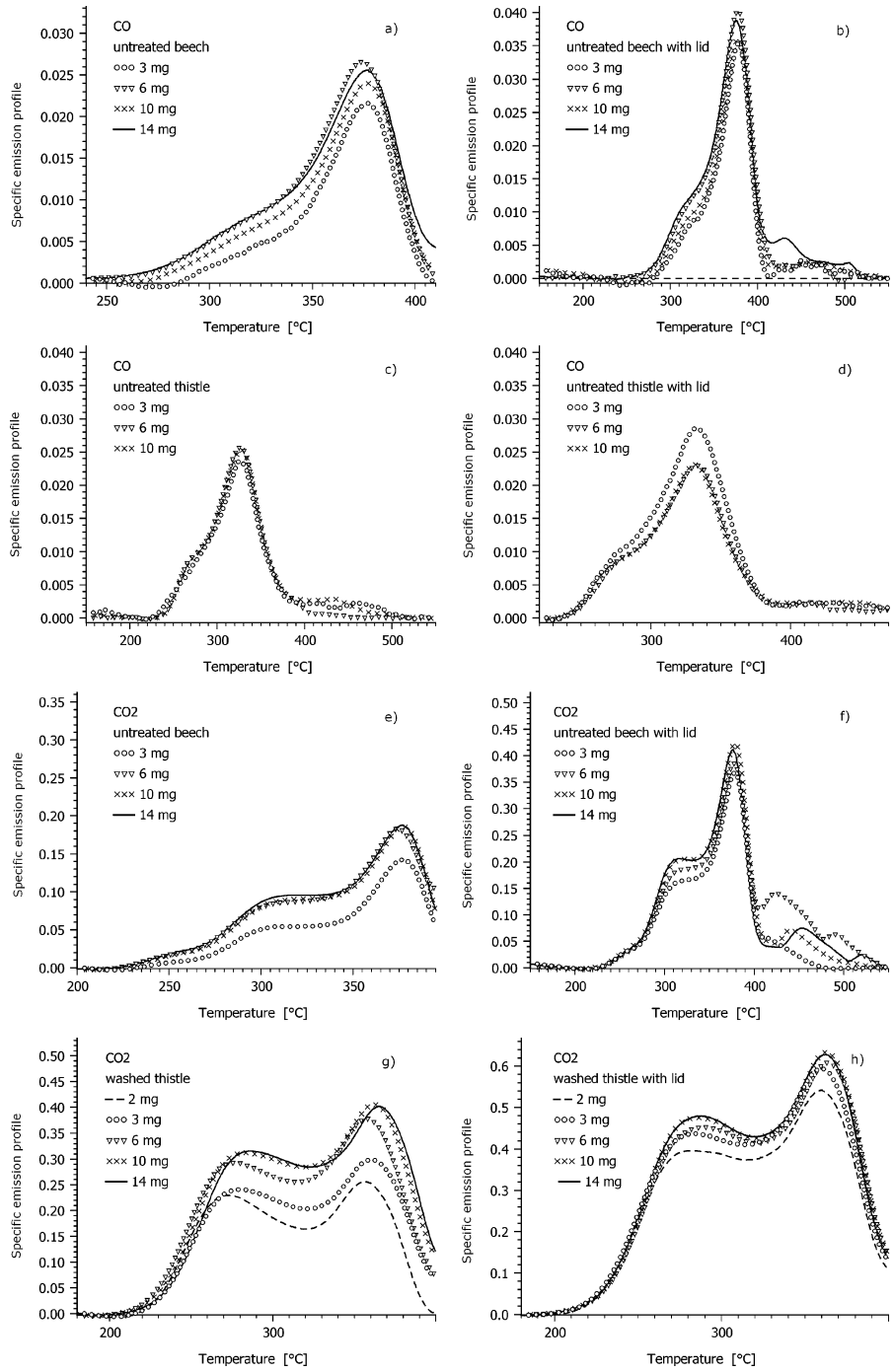

Figure 10. CO and CO_2 evolution profiles from untreated beech, untreated thistle, and washed thistle at 20 °C/min, using crucibles with and without lids. Results for samples having different initial weights are also reported. The scaling factors for the individual species evolved from wood and thistle are the same.

tion of 6 mg of each sample are compared (330 °C for untreated thistle, 361 °C for washed thistle, and 378 °C for untreated beech). The untreated thistle sample exhibits the lowest spectral absorbances associated with C═O and C─H stretching vibrations and the highest absorbances due to CO_2 release. This might be a result of the higher lignin content of this herbaceous crop, given that the evolution of organic compounds is expected to be considerably higher from polysaccharides than from lignin.[48,49] On the other hand, beech, the sample that exhibits the maximum rate of decomposition, shows correspondingly the highest C═O and C─H absorptions. The volatile organic production from the thistle becomes closer to that from beech as a result of the water-washing pretreatment. At the same time, the CO_2 production is still considerably higher in the decomposition of the washed thistle sample, as shown in Figure 7A. The larger CO_2 production from the thistle samples can be attributed to the specific structural feature of the lignin present in this biomass. From a lignin with high γ-COOH and γ-COOR group contents, carboxyl groups are preferably eliminated through the release of carbon dioxide.[50]

The use of covered pans appeared to modify the release of some of the volatile products, as shown by a comparison of parts A and B of Figure 7. Absorption due to C═O and C─H stretching decreases for all of the samples in the presence of a lid, whereas the CO_2 production from beech increases, becoming roughly equal to that of the thistle samples. The higher quantities of CO_2 and CO formed in the presence of a lid might be caused by the enhancement of secondary decomposition reactions of

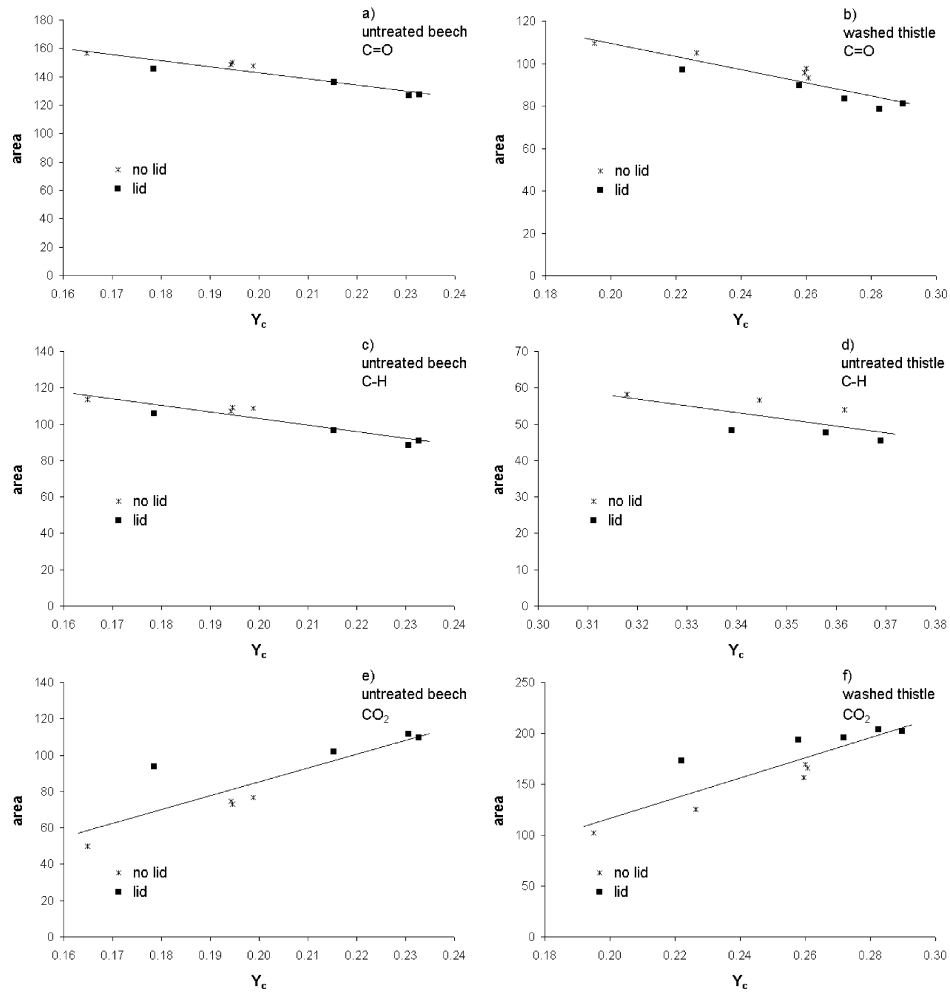

Figure 11. FTIR areas from the evolution profiles of biomass pyrolysis products at 20 °C/min, as a function of the char yield, obtained using crucibles with and without lids.

the volatiles, due to the increased residence time of these compounds in the vicinity of the solid residue. Thus, the results of evolved gas analysis confirm that closed vessel conditions enhance secondary exothermic reactions of the volatiles.

Figure 8 compares the differential thermogravimetric curve and the evolution profiles obtained in experimental runs carried out in crucibles with and without lids, in the temperature ranges corresponding to the main decomposition domain. The specific emission profiles reported in this figure were obtained following the procedure outlined in section 2.4, with the results normalized by the initial sample mass. As expected, a strong correspondence was observed between the product evolution profiles and the weight loss behavior of each sample.

Figures 9 and 10 report the specific emission profiles recorded for the different samples. It is evident from these figures that the increase in the initial sample mass and the use of covered pans entail a decrease in the production of organic compounds (see the C═O and C—H profiles in Figure 9). A decrease in the evolution of carbonyl functionalities from the shoulder associated with hemicellulose was also observed in the case of beech when higher initial sample weights were used (see Figure 9a,b).

The use of both higher sample masses and covered pans leads to an increase in carbon dioxide production (Figure 10). As discussed earlier, prolonged vapor-phase residence times of the primary pyrolysis products likely enhance secondary reactions yielding carbon dioxide and char.

A more complex behavior is shown in Figure 10 by carbon monoxide. A first mechanism of CO evolution is from the large number of hydroxyl groups and oxygen atoms present in the natural polymers that make up the cell walls. This pattern of evolution thus is simultaneous with the release of organic compounds. On the other hand, carbon monoxide is one of the cracking products from the char formation reactions. Consequently, additional quantities of CO can be formed from enhanced secondary interactions. The presence of these two patterns of CO evolution can explain the trends of CO formation observed in Figure 10.

To assess the specific trends in the yields of the different pyrolysis products, the integral in eq 7 was calculated for the chemical species listed in Table 2 in the temperature range corresponding to the main decomposition domain. The results obtained (normalized by the initial sample mass) are plotted in Figure 11 as a function of char yield. The figure shows that a roughly linear relation is present between the yields of the different volatile products and the char yield, particularly for organic compounds and carbon dioxide: a decrease in the production of organics and an increase in the global amount of CO_2 formed are associated to higher char yields. These results seem to confirm that a higher time of contact between primary volatiles and the solid residue causes secondary exothermic reactions that lead to the production of additional CO_2 and char.

4. Conclusions

The thermal effects of the primary pyrolysis process were investigated for a wood and an herbaceous biomass sample. As expected, the higher lignin content of the herbaceous crop resulted in a higher exothermicity for its overall decomposition process. Sample pretreatments, such as extraction and water washing, progressively shifted the overall thermal effects of the primary decomposition toward endothermicity. Secondary interactions among primary volatiles and the solid residue were shown to have a major role in the overall thermal effects of the pyrolysis process. The results of specific DSC runs and of TG-DSC-FTIR analysis indicated that the enhancement of the contact time between the volatiles and the primary char causes strongly exothermic secondary reactions, resulting in the formation of secondary char and an increase in carbon dioxide formation. Linear relations were found between the final char yield, the overall reaction heat, and the CO_2 formation, leading to significant modifications in the final yields and in the thermal effects of the pyrolysis process. Secondary reactions were shown to strongly affect the overall thermal effects of the process, which can shift from endothermic to exothermic in the case of the wood samples, if a sufficient contact time between the volatiles and the primary char is allowed in the pyrolysis system.

Nomenclature

A = absorbance
c = concentration (mol L^{-1})
$c_{p,bio}$ = specific heat of biomass (J g^{-1} K^{-1})
$c_{p,char}$ = specific heat of char (J g^{-1} K^{-1})
D = integral of I with respect to time (cm^{-1} s)
DTG = differential weight loss curve (s^{-1})
H_{total} = total heat of pyrolysis (J g^{-1})
I = integrated absorbance (cm^{-1})
K = experimental correlation factor relating I to concentration (cm^{-1} mol^{-1} L)
l = optical path length (cm)
m_0 = initial weight of sample, dry (g)
m_{char} = weight of char sample, dry (g)
m_T = sample weight at temperature T, dry (g)
Q = heat flow (general) for the representation in the figures (mW, mW/mg)
$Q_{bio,s}$ = calculated heat flow for the heating of biomass (W)
Q_{char} = experimental heat flow from the residual char (W)
$Q_{char,s}$ = calculated heat flow for the heating of char (W)
Q_r = heat flow induced by the pyrolysis reaction (W)
Q_{rad} = heat flow due to heat radiation effects in the DSC instrument (W)
Q_{run} = experimental heat flow from the biomass sample (W)
Q_s = calculated heat flow for the heating of the pyrolyzing solid sample taking into account the transition from biomass to char (W)
t = time (s)
T = temperature (°C, K)
T_1 = temperature of start of decomposition (K)
T_2 = temperature of end of decomposition (K)
X = conversion of the sample related to the dry sample mass
Y_c = char fraction at 550 °C
ε = extinction coefficient (cm^{-1} mol^{-1} L)
$\tilde{\nu}$ = wavenumber (cm^{-1})

Literature Cited

(1) Klass, D. L. *Biomass for Renewable Energy, Fuels, and Chemicals*; Academic Press: San Diego, CA, 1998.

(2) Bridgwater, A. V., Ed. *Pyrolysis and Gasification of Biomass and Waste*; CPL Press: Newbury, U.K., 2003.

(3) Bridgwater A. V., Boocock, D. G. B., Eds. *Science in Thermal and Chemical Biomass Conversion*; CPL Press: Newbury, U.K., 2006.

(4) Bridgwater, A. V.; Toft, A. J.; Brammer, J. G. A techno-economic comparison of power production by biomass fast pyrolysis with gasification and combustion. *Renewable Sustainable Energy Rev.* **2002**, *6*, 181.

(5) Bridgwater, A. V. Renewable fuels and chemicals by thermal processing of biomass. *Chem. Eng. J.* **2003**, *91*, 87.

(6) Bridgwater, A. V. Review: Biomass for Energy. *J. Sci. Food Agric.* **2006**, *86*, 1755.

(7) Bridgwater, A. V. The production of biofuels and renewable chemicals by fast pyrolysis of biomass. *Int. J. Global Energy Issues* **2007**, *27*, 160.

(8) Brammer, J. G.; Lauer, M.; Bridgwater, A. V. Opportunities for biomass-derived "bio-oil" in European heat and power markets. *Energy Policy* **2006**, *34*, 2871.

(9) Berndesa, G.; Hoogwijkb, M.; Van Den Broek, R. The contribution of biomass in the future global energy supply: A review of 17 studies. *Biomass Bioenergy* **2003**, *25*, 1.

(10) Yaman, S. Pyrolysis of biomass to produce fuels and chemical feedstocks. *Energy Convers. Manage.* **2004**, *45*, 651.

(11) Demirbas, M. F.; Balat, M. Biomass pyrolysis for liquid fuels and chemicals: A review. *J. Sci. Ind. Res.* **2007**, *66*, 797.

(12) Babu, B. V. Biomass pyrolysis: A state-of-the-art review. *Biofuels, Bioprod. Biorefin.* **2008**, *2*, 393.

(13) Di Blasi, C.; Russo, G. Modeling of transport phenomena and kinetics of biomass pyrolysis. In *Advances in Thermochemical Biomass Conversion*; Bridgwater, A. V., Ed.; Blackie Academic and Professional: London, 1994; Vol. 2, pp 906−921.

(14) Di Blasi, C. Comparison of semi-global mechanisms for primary pyrolysis of lignocellulosic fuels. *J. Anal. Appl. Pyrolysis* **1998**, *47*, 43.

(15) Di Blasi, C.; Branca, C.; Santoro, A.; Bermudez, R. A. P. Weight loss dynamics of wood chips under fast radiative heating. *J. Anal. Appl. Pyrolysis* **2001**, *57*, 77.

(16) Di Blasi, C.; Branca, C.; Santoro, A.; Hernandez, E. G. Pyrolytic behaviour and products of some wood varieties. *Combust. Flame* **2001**, *124*, 165.

(17) Di Blasi, C. Modeling of chemical and physical processes of wood and biomass pyrolysis. *Prog. Energy Combust. Sci.* **2008**, *34*, 47.

(18) Miller, R. S.; Bellan, J. A generalized biomass pyrolysis model based on superimposed cellulose, hemicellulose and lignin kinetics. *Combust. Sci. Technol.* **1997**, *126*, 97.

(19) Manyà, J. J.; Velo, E.; Puigjaner, L. Kinetics of biomass pyrolysis: A reformulated three-parallel-reactions model. *Ind. Eng. Chem. Res.* **2003**, *42*, 434.

(20) Babu, B. V.; Chaurasia, A. S. Modelling for pyrolysis of solid particle: Kinetics and heat transfer effects. *Energy Convers. Manage.* **2003**, *44*, 2251.

(21) Kersten, S.; Wang, X.; Prins, W.; Swaaij, W. Biomass pyrolysis in a fluidized bed reactor. Part 1: Literature review and model simulations. *Ind. Eng. Chem. Res.* **2005**, *44*, 8773.

(22) Radmanesh, R.; Courbariaux, Y.; Chaouki, J.; Guy, C. A unified lumped approach in kinetic modeling of biomass pyrolysis. *Fuel* **2006**, *85*, 1211.

(23) Schröder, E.; Thomauske, K.; Weber, C.; Hornung, A.; Tumiatti, V. Experiments on the generation of activated carbon from biomass. *J. Anal. Appl. Pyrolysis* **2007**, *79*, 106.

(24) Dente, M.; Bozzano, G.; Faravelli, T.; Marongiu, A.; Pierucci, S.; Ranzi, E. Kinetic Modelling of Pyrolysis Processes in Gas and Condensed Phase. *Adv. Chem. Eng.* **2007**, *32*, 51.

(25) Ranzi, E.; Cuoci, A.; Faravelli, T.; Frassoldati, A.; Migliavacca, G.; Pierucci, S.; Sommariva, S. Chemical Kinetics of Biomass Pyrolysis. *Energy Fuels* **2008**, *22*, 4292.

(26) Balat, M. Mechanisms of thermochemical biomass conversion processes. Part 1: Reactions of pyrolysis. *Energy Sources A* **2008**, *30*, 620.

(27) Dupont, C.; Commandre, J.-M.; Gauthier, P.; Boissonnet, G.; Salvador, S.; Schweich, D. Biomass pyrolysis experiments in an analytical entrained flow reactor between 1073K and 1273K. *Fuel* **2008**, *87*, 1155.

(28) Ghabi, C.; Benticha, H.; Sassi, M. Two-Dimensional Computational Modeling and Simulation of Wood Particles Pyrolysis in a Fixed Bed Reactor. *Combust. Sci. Technol.* **2008**, *180*, 833.

(29) Khalil, R. A.; Mészáros, E.; Grønli, M. G.; Várhegyi, G.; Mohai, I.; Marosvölgyi, B.; Hustad, J. E. Thermal analysis of energy crops: Part I: The applicability of a macro-thermobalance for biomass studies. *J. Anal. Appl. Pyrolysis* **2008**, *81*, 52.

(30) Lappas, A. A.; Dimitropoulos, V. S.; Antonakou, E. V.; Voutetakis, S. S.; Vasalos, I. A. Design, Construction, and Operation of a Transported

Fluid Bed Process Development Unit for Biomass Fast Pyrolysis: Effect of Pyrolysis Temperature. *Ind. Eng. Chem. Res.* **2008**, *47*, 742.

(31) Van de Velden, M.; Baeyens, J.; Boukis, I. Modeling CFB biomass pyrolysis reactors. *Biomass Bioenergy* **2008**, *32*, 128.

(32) Antal, M. J.; Grønli, M. The art, science, and technology of charcoal production. *Ind. Eng. Chem. Res.* **2003**, *42*, 1619.

(33) Rath, J.; Wolfinger, M.; Steiner, G.; Krammer, G.; Barontini, F.; Cozzani, V. Heat of wood pyrolysis. *Fuel* **2003**, *82*, 81.

(34) Buekens, A. G.; Bridgwater, A. V.; Ferrero, G. L.; Maniatis, K. *Commercial and Marketing Aspects of Gasifiers*; EUR 12736; Commission of the European Communities: Brussels, Belgium, 1990.

(35) McKendry, P. Energy production from biomass (part 3): Gasification technologies. *Bioresour. Technol.* **2002**, *83*, 55.

(36) Antal, M. J.; Várhegyi, G. Cellulose pyrolysis kinetics: The current state of knowledge. *Ind. Eng. Chem. Res.* **1995**, *34*, 703.

(37) Mok, W.S.-L.; Antal, M. J.; Szabo, P.; Várhegyi, G.; Zelei, B. Formation of charcoal from biomass in a sealed reactor. *Ind. Eng. Chem. Res.* **1992**, *31*, 1162.

(38) Várhegyi, G.; Jakab, E.; Till, F.; Székely, T. Thermogravimetric−mass spectrometric characterization of the thermal decomposition of sunflower stem. *Energy Fuels* **1989**, *3*, 755.

(39) DeGroot, W. F.; Pan, W.-P.; Rahman, M. D.; Richards, G. N. First chemical events in the pyrolysis of wood. *J. Anal. Appl. Pyrolysis* **1988**, *13*, 221.

(40) Várhegyi, G.; Grønli, M. G.; Blasi, C. D. Effects of sample origin, extraction, and hot-water washing on the devolatilization kinetics of chestnut wood. *Ind. Eng. Chem. Res.* **2004**, *43*, 2356.

(41) Gómez, C. J.; Manyà, J. J.; Velo, E.; Puigjaner, L. Further applications of a revisited summative model for kinetics of biomass pyrolysis. *Ind. Eng. Chem. Res.* **2004**, *43*, 901.

(42) Gómez, C. J.; Várhegyi, G.; Puigjaner, L. Slow pyrolysis of woody residuals and an herbaceous biomass crop: A kinetic study. *Ind. Eng. Chem. Res.* **2005**, *44*, 6650.

(43) Wolfinger, M. G.; Rath, J.; Krammer, G.; Barontini, F.; Cozzani, V. Influence of the emissivity of the sample on differential scanning calorimetry measurements. *Thermochim. Acta* **2001**, *372*, 11.

(44) Barontini, F.; Cozzani, V.; Petarca, L. Thermal stability and decomposition products of hexabromocyclododecane. *Ind. Eng. Chem. Res.* **2001**, *40*, 3270.

(45) Marsanich, K.; Barontini, F.; Cozzani, V.; Petarca, L. Advanced pulse calibration techniques for the quantitative analysis of TG-FTIR data. *Thermochim. Acta* **2002**, *390*, 153.

(46) Stenseng, M.; Jensen, A.; Dam-Johansen, K. Investigation of biomass pyrolysis by thermogravimetric analysis and differential scanning calorimetry. *J. Anal. Appl. Pyrolysis* **2001**, *765*, 58–59.

(47) Biagini, E.; Barontini, F.; Tognotti, L. Devolatilization of Biomass Fuels and Biomass Components Studied by TG/FTIR Technique. *Ind. Eng. Chem. Res.* **2006**, *45*, 4486.

(48) Evans, R. J.; Milne, T. A. Molecular characterization of the pyrolysis of biomass. 1. Fundamentals. *Energy Fuels* **1987**, *1*, 123.

(49) Mészáros, E.; Jakab, E.; Várhegyi, G.; Szepesváry, P.; Marosvölgyi, B. Comparative study of the thermal behavior of wood and bark of young shoots obtained from an energy plantation. *J. Anal. Appl. Pyrolysis* **2004**, *72*, 317.

(50) Jakab, E.; Faix, O.; Till, F. Thermal decomposition of milled wood lignins studied by thermogravimetry/mass spectrometry. *J. Anal. Appl. Pyrolysis* **1997**, *40−41*, 171.

Received for review May 16, 2009
Revised manuscript received September 22, 2009
Accepted October 5, 2009

IE9007985